PAPER

Check for updates

An esterase-activatable prodrug formulated liposome strategy: potentiating the anticancer therapeutic efficacy and drug safety†

Linlin Shi,‡[ab] Xinkai Wu,‡[b] Tongyu Li,[c] Yuan Wu,[d] Liwei Song,[e] Wei Zhang,[b] Luxi Yin,[b] Yuhui Wu,[b] Weidong Han [iD] *[ab] and Yunhai Yang*[e]

Liposomal nanomedicine represents a common and versatile carrier for the delivery of both lipophilic and hydrophilic drugs. However, the direct formulation of many chemotherapeutics into a liposomal system remains an enormous challenge. Using the topoisomerase I inhibitor 7-ethyl-10-hydroxycamptothecin (SN38) as a model drug, we combined lipophilic prodrug construction with subsequent integration into an exogenous liposomal scaffold to assemble a prodrug-formulated liposome for systemic administration. Reconstructing SN38 with lipid cholesterol *via* the esterase-activatable bond endows the resulting prodrug with elevated miscibility with liposomal compositions and esterase-responsive drug release in cancerous cells. The systemic administration of the prodrug-based nanoassemblies (**Chol-SN38@LP**) exhibited preferential accumulation of therapeutic payloads in tumor lesions. Compared to the SN38 clinical counterpart irinotecan, our prodrug-based nanoassemblies with adaptive features showed elevated therapeutic efficacy (∼1.5 times increase of tumor inhibition) in a preclinical A549 lung carcinoma cell-derived mouse model and improved drug tolerability (*i.e.*, alleviated bloody diarrhea and liver damage) in multiple mice models. These results may be ascribed to extended systemic circulation and preferential tumor accumulation of our nanodrugs. Hence, our findings demonstrate that rational engineering of therapeutic nanomedicine is a promising approach for effective and safe delivery of antitumor chemotherapeutics, especially to rescue drug candidates that have failed in clinical trials owing to poor PK properties or severe toxicity in patients.

1. Introduction

SN38 (7-ethyl-10-hydroxycamptothecin), an active metabolite of irinotecan (CPT-11), is a potent inhibitor of DNA topoisomerase I.[1–3] SN38 exhibits 100- to 1000-fold higher potency than its prodrug CPT-11 against a broad spectrum of cancer in *in vitro* cytotoxicity tests.[4,5] In the body, only a small percentage of CPT-11 is hepatically metabolized and converted to active SN38 (2–8%) due to its low carboxyl esterase (CES) substrate affinity.[6,7] In

aCancer Institute (Key Laboratory of Cancer Prevention and Intervention, China National Ministry of Education), 2nd Affiliated Hospital, School of Medicine, Zhejiang University, Hangzhou, Zhejiang, PR China, 310009

bDepartment of Medical Oncology, Sir Run Run Shaw Hospital, School of Medicine, Zhejiang University, Hangzhou, PR China, 310016. E-mail: hanwd@zju.edu.cn

cDepartment of Hematology, Ningbo First Hospital, Ningbo, Zhejiang, PR China, 315010

dDepartment of Respiratory Medicine, The Fourth Affiliated Hospital, College of Medicine, Zhejiang University, Yiwu, Zhejiang, PR China, 310014

eShanghai Pulmonary Tumor Medical Center, Shanghai Chest Hospital Affiliated to Shanghai Jiaotong University, Shanghai, PR China, 200030. E-mail: docyyh@163.com

† Electronic supplementary information (ESI) available. See DOI: 10.1039/d1na00838b

‡ These authors contributed equally to this work.

addition, in the clinics, less than 1% of the total injected dose of CPT-11 reaches tumors because of nonspecific distribution as well as rapid metabolism and clearance.[8] As a result, we can reasonably envision that the SN38 agent could be directly utilized to develop alternative SN38 drugs or related nano-formulations to boost premium therapeutic outcomes, thus bypassing the side effects elicited by inefficient activation and nonspecific dissemination of CPT-11.

Liposomes, as conventional and biocompatible drug delivery systems, have special capacities to increase drug loading (DL) and encapsulation efficiency (EE) of both lipophilic and hydrophilic drugs.[9–11] Compared with free formulations, pharmaceutical delivery with liposomes significantly increases the pharmacokinetics (PK) of drugs. Many liposome-formulated chemotherapeutics have entered the market (*e.g.*, Doxil®, Marqibo®)[12,13] or are in clinical trials (*e.g.*, Arikace™, Stimuvax®)[14,15] for cancer therapy. We thus are interested in the liposomal strategy for potent and safe *in vivo* delivery of SN38. Unfortunately, assembling parent SN38 into conventional liposome scaffolds poses a formidable challenge, presumably due to the intrinsically planar structure and moderate polarity of this therapeutic agent.[2,5] In addition, the burst release of simply physically encapsulated drugs upon systemic

administration could cause suboptimal PK properties as well as undesired efficacy and safety.[16,17] Therefore, rational chemical modification of this molecule to enable self-assembly or coassembly with other matrices is plausible to address the above intractable challenges.

Previous studies have demonstrated that the conjugation of drugs with lipid cholesterol could substantially augment their miscibility with liposomal matrices, thus enhancing efficient cellular uptake and alleviating the side effects of drugs.[18–20] Inspired by these efforts, we chose cholesterol to generate a new

chemical derivative of SN38 for subsequent generation of prodrug-encapsulated liposomes (Fig. 1). Succinic anhydride was utilized to esterify the hydroxyl moieties on SN38 and cholesterol for the reconstitution of conjugate **Cholesterol-SN38** (**Chol-SN38**). The diester bonds in the conjugate confer the resulting liposomes with hypersensitivity to the abundant esterase in cancerous cells but are kept blunt during blood circulation, which helps to release active SN38 and exert tumoricidal activity.

Furthermore, to stably constrain cargos within the liposomal carrier and reduce their clearance in the blood, we formulated
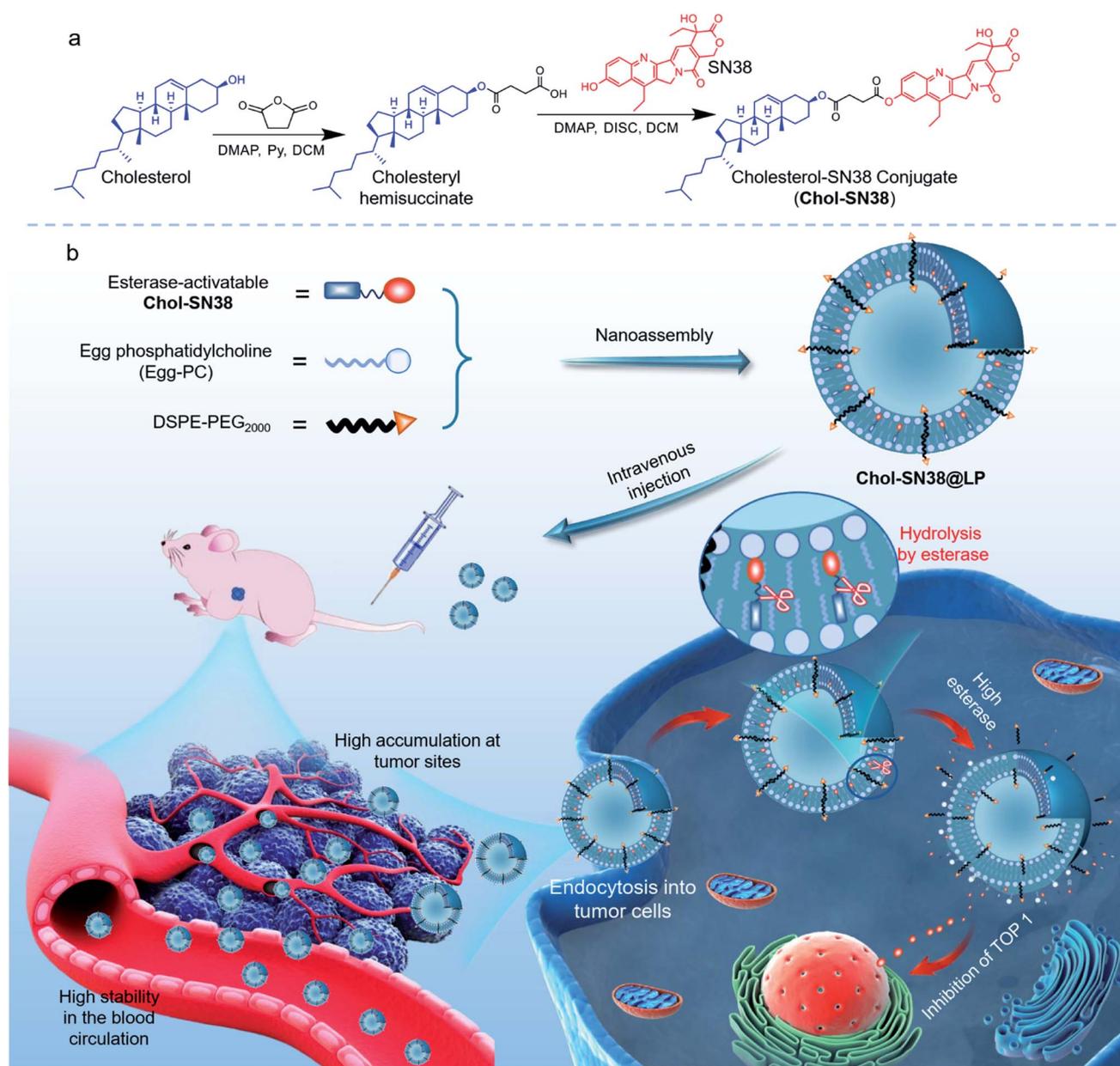

Fig. 1 Schematic illustration of the preparation of esterase-activatable prodrug-based nanoparticles for efficient, potent and safe *in vivo* delivery in the treatment of lung malignancies. (a) Chemical synthesis of esterase-sensitive prodrug **Chol-SN38**. (b) *In vivo* delivery of prodrug-based liposomes in tumor-bearing mice and the esterase-responsive hydrolysis of liposomes in cancerous cells. SN38 prodrug **Chol-SN38** coassembles with liposomal compositions to formulate **Chol-SN38@LP**. The nanomedicines maintain high stability in the blood circulation and efficiently accumulate in tumor sites *via* passive targeting. Once internalized into tumor cells and hydrolyzed by high concentrations of esterase inside tumor cells, liposomes released active SN38 to inhibit TOP 1 for DNA damage.

liposomes with poly(ethylene glycol) (PEG) functionality.[21,22] With re-engineered architectures, the SN38 prodrug-based liposomal formulation (termed **Chol-SN38@LP**) demonstrated better therapeutic efficacy and safety profiles in multiple mouse models than clinically formulated CPT-11. In general, our findings proved this rationally designed, prodrug formulated, esterase-activatable drug delivery platform as a simple yet versatile paradigm for transforming highly toxic chemotherapeutic agents into efficacious liposomes for cancer treatment.

2. Materials and methods

Materials

SN38 was purchased from Knowshine Pharmachemicals Inc. (Shanghai, China). CPT-11 was purchased from Sigma Life Science (D2534-1G, USA). Cholesterol (Chol), egg phosphatidylcholine (Egg-PC) and 1,2-distaroyl-sn-glycero-3-phosphoethanolamine-N-[methoxy(polyethylene glycol)$_{2000}$] (DSPE-PEG$_{2000}$) were purchased from A.V.T. Pharmaceutical Co., Ltd. (Shanghai, China). DiI and DiR were purchased from Invitrogen Corporation (USA). All solvents were purchased from J&K Scientific (Shanghai, China). The BASO fecal OB-II assay kit was purchased from BASO Diagnostic Inc. (Zhuhai, China). Acridine orange/ethidium bromide (AO/EB) dual staining assay kits were purchased from Solarbio Science & Technology Co., Ltd. (Beijing, China). CCK-8 kits were purchased from MedChem Express (New Jersey, USA). EdU cell proliferation testing kits were purchased from RiboBio Co., Ltd. (Guangzhou, China).

Preparation of prodrug-loaded liposomes

Prodrug-formulated liposomes were prepared by an ethanol dilution method as reported by our previous study.[9,16] Briefly, **Chol-SN38** conjugate (2 mg of SN38 equiv.), 14 mg of lipid (Egg-PC plus cholesterol) and 2 mg of DSPE-PEG$_{2000}$ were dissolved in a mixture solution consisting of 0.8 mL of ethanol and 0.2 mL of N,N-dimethylformamide (DMF). The solution was incubated in water at 55 °C for 0.5 h and then added to 9 mL of deionized (DI) water under stirring at room temperature. The molar ratios of **Chol-SN38** versus cholesterol were 1 : 0, 1 : 1, 1 : 2 and 1 : 5 for **LP 1–4**.

In vitro drug release kinetics of Chol-SN38@LP

Briefly, 3 mL of prodrug formulated liposomes in phosphate buffered saline (PBS) or PBS containing 50 U mL^{-1} porcine liver esterase (PLE) were loaded into dialysis bags (molecular weight cutoff 7 kDa) against 15 mL of PBS (pH = 7.4) with 0.3% Tween 80. Dialysis bags were continuously and vigorously shaken in an incubator shaker with a fixed incubation temperature of 37 ± 0.5 °C. 1 mL release media was collected and supplemented with 1 mL of fresh medium at predetermined times. The collected medium was analyzed by UV-vis spectrometry measured at 378 nm.

Cell lines and cell culture

The human lung cancer cell lines A549 and PC-9, human colorectal cancer cell line LoVo and human breast cancer cell line MCF-7 were purchased from the cell bank of the Shanghai Chinese Academy of Sciences. All cells were cultured in Dulbecco's modified Eagle's medium (DMEM) supplemented with 10% fetal calf serum (FBS) and 1% penicillin/streptomycin and maintained in a humidified atmosphere with 5% CO$_2$ at 37 °C.

Phosphor-histone-H2A.X (γ-H2A.X) staining

A549 cells were seeded in 48-well plates and incubated overnight. The cells were treated with the same treatments as described above in the cell proliferation assay. Untreated cells were included as controls. The cells were then fixed with 4% paraformaldehyde for 30 min and permeated with 0.5% Triton X-100 for 1 h. The cells were next blocked with BSA and immunostained with γ-H2A.X antibody (Cell Signaling Technology Inc., USA) for 1 h at room temperature. The cells were then washed with PBS three times before being subsequently stained with Alexa Fluor® 488 (AF-488)-labeled secondary antibody (Life Technologies, USA) for 40 min at room temperature. After nuclear staining with DAPI for 20 min, the cells were imaged by a fluorescence microscope.

Cellular uptake analysis by confocal laser scanning microscopy (CLSM) and flow cytometry (FCM)

To trace the cellular uptake of liposomes, a fluorescence probe, DiI, was coassembled into **Chol-SN38@LP** (termed **DiI/SN38@LP**). A549 cells were seeded on confocal dishes at a cell density of 5×10^4 per dish. The cells were incubated overnight and administered 15 μg mL^{-1} DiI (DiI equivalent concentration)-loaded liposomes for an additional 2, 4 and 6 h at 37 °C. Prior to observation by FV3000 (Olympus, Japan), the cells were stained with Hoechst 33342 (blue) and LysoTracker green NDN-26 (green) for 15 min. The intracellular trafficking of liposomes was also detected by FCM. The cells were seeded on 12-well plates and allowed to attach overnight. After drug administration, the cells were collected and analyzed by FCM (Cytoflex LX, Beckman Coulter, USA).

Endocytic pathways of liposomes

In brief, A549 cells were seeded in 12-well plates at a cell density of 1×10^5 per well and incubated overnight. Before liposome administration, cells were incubated with chlorpromazine (15 μg mL^{-1}), cytochalasin D (60 μM) and filipin (5 μg mL^{-1}) for 1 h at 37 °C. Next, the inhibitors were removed and supplemented with 1 mL of **DiI/SN38@LP** for another 2 h of incubation. After incubation, cells were collected and analyzed by FCM (Cytoflex LX, Beckman Coulter, USA). To evaluate the uptake efficiency of liposomes at low temperature, cells were preincubated at 4 °C for 0.5 h before supplementation with DiI-loaded liposomes. Cells were then again kept at 4 °C for 2 h before collection for FCM. Cells not administered inhibitors but treated with liposomes and incubated at 37 °C were included as positive controls. The cells were seeded on confocal dishes and subjected to the same treatment with inhibitors and low-temperature preincubation as in FCM to analyze the endocytic pathway by CLSM.

Animal study

Mice were purchased from the Shanghai Experimental Animal Center, Chinese Academy of Sciences. All of the animal studies were approved by the Ethics Committee of the Zhejiang University School of Medicine and conducted in accordance with the National Institute Guide for the Care and Use of Laboratory Animals.

Ex vivo imaging study

To evaluate the drug distribution and tumor-targeting ability of prodrug-formulated liposomes, an A549 cell-derived xenograft mouse model was established by subcutaneous injection of 5×10^6 A549 cells into the right flanks of 4 week-old BALB/c nude mice. When the tumor size reached ~500 mm^3, the mice were randomly divided into two groups ($n = 8$). A near-infrared (NIR) fluorescence probe, DiR, was coassembled into the liposomes (termed **DiR/SN38@LP**) to track the *in vivo* distribution of the liposomes. The mice were injected with free DiR (dissolved in ethanol and diluted in DI water) and **DiR/SN38@LP** at a DiR dose of 14 μg per mouse *via* the tail vein. At both 24 h and 48 h, the mice ($n = 4$ in each group) were sacrificed to obtain tumors and organs for *ex vivo* imaging using an *in vivo* imaging system (IVIS Spectrum, USA). The tumors were then fixed with optimal cutting temperature compound (OCT) containing block holders for snap freezing. The tissue blocks were sectioned (8 μm) using a cryostat (CM1950, Leica, Germany). The cell nuclei were stained with DAPI (4,6-diamidino-2-phenylindole) for 20 min at room temperature before being observed by CLSM (FV3000, Olympus, Japan).

In vivo antitumor study

The A549 cell-derived xenograft mouse model was established as described above. When the tumor volume reached approximately 150 mm^3, the mice were randomly divided into 3 groups ($n = 8$). The intravenous administrations (days 0, 3, 6) to mice were as follows: saline, CPT-11 and **Chol-SN38@LP** (15 mg kg^{-1} at SN38 equiv.). The tumor size and body weight of mice in each group were recorded every three days. The tumor size was recorded and calculated by the formula: $V = (L \times W^2)/2$, in which W (width) is smaller than L (length). One representative tumor of each group was extracted on Day 9 for histological analysis, including H&E, immunohistochemistry (IHC), Ki-67 and p-H2A.X, HUABIO) and immunofluorescent (IF, TUNEL) staining. At the end of observation (day 30), all mice were sacrificed to collect tumors and measure tumor weights.

Evaluation of *in vivo* drug toxicity

ICR mice (5 weeks old, $n = 8$ per group) were given three injections of CPT-11 and **Chol-SN38@LP** at 15 mg kg^{-1} SN38 equiv. dose every other day. Mice treated with saline were included as controls. The severity of bloody diarrhea was monitored by a BASO fecal OB-II kit according to the manufacturer's protocol on days 2, 4, 6 and 7.[4,5] Organs, including the liver, heart, lung, spleen, kidney and ileum, were collected from mice on day 7 to further assess the side effects of **Chol-**

SN38@LP in mouse organs. Blood samples ($n = 6$ per group) were also collected at 7 days post administration to evaluate hepatorenal toxicity. Serum was extracted from blood samples and tested for hepatorenal parameters, including aspartate aminotransferase (AST), alanine aminotransferase (ALT), total bilirubin (TBIL), blood urea nitrogen (BUN) and creatinine (CR).

Statistical analysis

All quantitative data are presented as the mean ± standard deviation (SD) of three independent experiments. Statistical significance was evaluated using a two-tailed unpaired Student's *t*-test with SPSS 17.0 software. The threshold for statistical significance was *$p < 0.05$; **$p < 0.01$; ***$p < 0.001$.

3. Results

3.1. Synthesis and characterization of esterase-activatable SN38 prodrug

To facilitate the synthesis of prodrug and achieve desirable drug loading as well as high miscibility of prodrug in liposomes, we chose cholesterol (an essential component widely used in formulating liposomes) for drug derivatization. Furthermore, we chose succinic anhydride for the conjugation of cholesterol and SN38 to achieve potent esterase-activatable prodrugs, which we abbreviated as **Chol-SN38**. The convergent chemical synthesis of **Chol-SN38** is presented in Fig. 1a. Succinic acid was first conjugated to cholesterol to form cholesteryl hemisuccinate under pyridine and DMAP. The final compound **Chol-SN38** was produced by reacting cholesteryl hemisuccinate with SN38 under the catalysis of DMAP and DISC. The products in each procedure were obtained with high yields (above 83%) after chromatographic purification. Characterization of cholesteryl hemisuccinate and **Chol-SN38** with ^{1}H nuclear magnetic resonance (NMR) spectroscopy revealed the successful synthesis of the desired adducts (Fig. S1 and S2†). The exact correct molecular weight from the mass spectrum (Fig. S3†) of **Chol-SN38** further agreed well.

3.2. Assembly of Chol-SN38 into liposomal delivery vehicles and characterization

We hypothesized that the conjugation of cholesterol with drugs could enhance the lipophilicity of the prodrugs and the miscibility with liposomal scaffolds, thereby stabilizing them in the lipid bilayers of liposomal formulations. To reduce blood clearance in the reticuloendothelial system (RES) and elongate the circulation time of liposomes, we formulated liposomes with PEG functionality. We therefore planned to assemble prodrug-formulated liposomes with chemical compositions including Egg-PC, cholesterol and DSPE-PEG$_{2000}$ to achieve effective drug delivery, as shown in Fig. 1b. By altering the molar ratio of **Chol-SN38** *versus* cholesterol, we prepared four liposomes, designated **LP 1** (1 : 0), **LP 2** (1 : 1), **LP 3** (1 : 2), and **LP 4** (1 : 5). As indicated in Fig. S4,† the resulting liposome **LP 1** had the highest transparency, implying the smallest particle size. Morphological observation of these four liposomes by transmission electron microscopy (TEM) visualization revealed
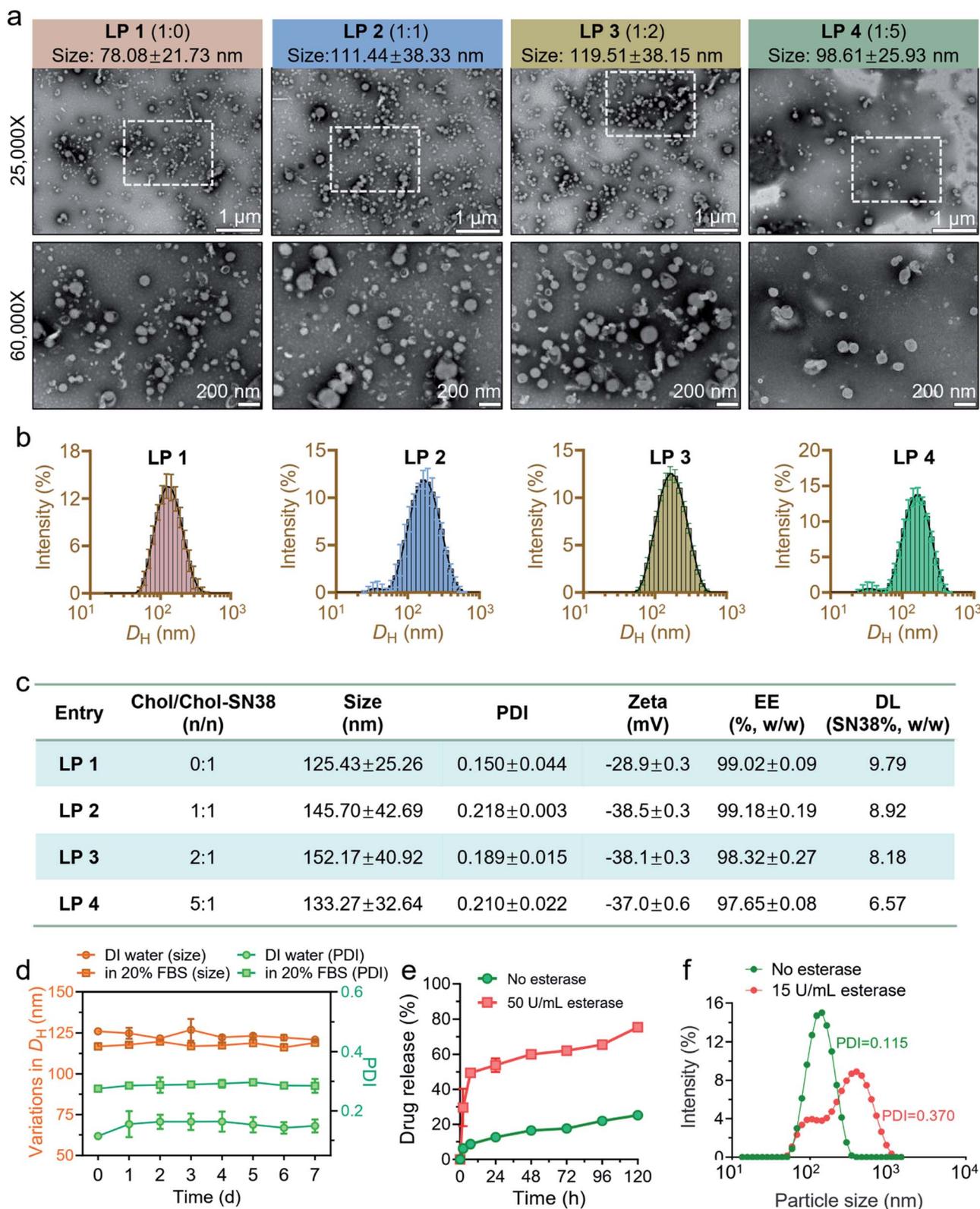
Fig. 2 Characterization and optimization of liposomes. (a) Transmission electron microscopy (TEM) images of four liposomes. According to the molar ratio of cholesterol *versus* **Chol-SN38**, 0 : 1, 1 : 1, 2 : 1 and 5 : 1, liposomes were designated **LP 1**, **LP 2**, **LP 3** and **LP 4**, respectively. (b) Size distribution of the prodrug-loaded liposomes measured by dynamic light scattering. (c) Characterization features of liposomes, including particle size, PDI, zeta potential, encapsulation efficiency (EE) and drug loading (DL). (d) The colloidal stability of **LP 1** was evaluated in deionized (DI) water and phosphate buffered saline (PBS) containing 20% fetal calf serum (FBS) for 7 d by recording the variations in particle size and PDI. (e) *In vitro* drug release profiles from **LP 1** coincubated with or without 50 U mL^{-1} porcine liver esterase (PLE). (f) The size distribution of **LP 1** coincubated with or without 15 U mL^{-1} PLE for 48 h.

a characterized liposomal bilayer structure and nanoscale size (Fig. 2a). TEM results showed that the size of **LP 1** (78.08 ± 21.73 nm) was indeed smaller than that of the other three liposomes (approximate 100 nm). Dynamic light scattering (DLS) analysis confirmed again that the hydrodynamic diameters (D_H) of **LP 2**, **LP 3** and **LP 4** were larger than that of **LP 1** (Fig. 2b). Moreover, the **LP 1** formulation exhibited a relatively lower polydispersity index (PDI) than the other liposomes, as demonstrated by the monomodal distribution of this formulation (Fig. 2b and c).

The physicochemical properties, including zeta potential, EE and DL, of drugs were also characterized (Fig. 2c). The zeta potential of **LP 1** was −28.9 ± 0.3 mV, which was less negative potential than that of the other three liposomal formulations. In addition, the EE% of **LP 1** was determined to be 99.02 ± 0.09, which is similar to **LP 2** and slightly higher than that of **LP 3** and **LP 4**. Furthermore, without extra supplementation of parent cholesterol for liposome formulation, **LP 1** exhibited the highest DL among the four formulations. In conclusion, **LP 1** (hereafter termed **Chol-SN38@LP**) was chosen for further *in vitro* and *in vivo* drug demonstrations due to its superior physicochemical properties compared to the other three liposomal formulations in terms of size, EE and DL.

3.3. The stability and *in vitro* release kinetics of Chol-SN38@LP

The capability of liposomes to maintain their size in the serum ensures efficient drug accumulation at tumor lesions by the EPR effect during circulation.[23,24] As shown in Fig. 2d, no apparent variations in diameters or PDI values were observed during a 1 week incubation of **Chol-SN38@LP** in DI water and PBS containing 20% FBS, proving the excellent colloidal stability of the nanodrug.

Given that the drug conjugate **Chol-SN38** is formed *via* diester bonds, we explored that whether drug release would be accelerated upon incubation with esterase, which is abundant in tumor cells. As shown in Fig. 2e, the release of active SN38 was indeed remarkably accelerated in the presence of 50 U mL^{-1} PLE. Upon 24 h exposure to PLE, approximately 54% of the encapsulated drug was released from **Chol-SN38@LP**, which is approximately 4.3 times faster than controlled spontaneous drug release. In addition, we observed that the lower dose of PLE (15 U mL^{-1}) could also induce apparent variations in the particle size distribution of **Chol-SN38@LP** by DLS measurements, implying rapid structural disruption by esterase (Fig. 2f).

3.4. *In vitro* cytotoxicity of Chol-SN38@LP

We next evaluated the cytotoxicity of **Chol-SN38@LP** against A549, PC-9, LoVo and MCF-7 cells by measuring the half-maximal inhibitory concentration (IC$_{50}$) of cell proliferation in 72 h CCK-8 assays. CPT-11 and free SN38 were included as controls in this experimental setting. As shown in Fig. 3a–d, **Chol-SN38@LP** showed slightly less cytotoxicity in all cells than the free form of SN38, which could be attributed to the delayed release of the therapeutically active agent from the assembled liposomes. However, prodrug-based SN38 liposomes significantly increased the cytotoxicity to tumor cells in comparison

with CPT-11, as evidenced by an approximately 15 to 100-fold decrease in the IC$_{50}$ value. The increased cytotoxicity of **Chol-SN38@LP** might be ascribed to the efficient esterase-catalyzed hydrolysis and production of SN38 in tumor cells, whereas the conversion efficiency of CPT-11 to generate the metabolite SN38 is less than 8% due to low substrate affinity.[6,7] An EdU cell proliferation assay (Fig. 3e and f) also indicated that **Chol-SN38@LP** exerted a stronger inhibitory effect on cell proliferation than CPT-11 in A549 cells ($p < 0.001$).

The cell apoptosis and cell cycle distribution of A549 cells were investigated to further elucidate the *in vitro* cytotoxicity of **Chol-SN38@LP**. As indicated in Fig. 3g and h, both free SN38 and **Chol-SN38@LP** induced at least 1.6-fold higher apoptotic rate than that induced by CPT-11. Further analysis of the cell cycle indicated that relative to control or CPT-11-treatment, **Chol-SN38@LP** and free SN38 resulted in substantially higher G2/M phase arrest (Fig. 3i and j). These results explained that the cell proliferation inhibition and cell apoptosis in A549 cells caused by **Chol-SN38@LP** were probably attributed to cell cycle arrest at the G2/M stage.

We further explored whether the cytotoxicity of prodrug-based liposomes was achieved by inducing DNA damage. It is known that the chemotherapeutic SN38 is an inhibitor of DNA topoisomerase I, thus inhibiting DNA unwinding and inducing DNA damage.[25,26] A common view is that histone phosphorylation takes place *in situ* in damaged DNA,[27,28] implying that the expression of phosphorylated H2A.X (γ-H2A.X) is an indicator of DNA damage. We tested the expression level of γ-H2A.X by IF staining after 24 h of administration of drugs in various forms. As shown in Fig. 3k and l, **Chol-SN38@LP**- and free SN38-treated A549 tumor cells exhibited DNA damage as revealed by apparent H2A.X phosphorylation (42% and 44%, respectively), which are approximately 2 times higher than that induced by CPT-11. These data suggest that the elevated apoptosis was a result of the increased DNA damage in cancerous cells.

3.5. Cellular uptake and uptake mechanism of SN38 prodrug-based liposomes

To further explore the cellular uptake efficiency and mechanism of prodrug-based liposomes when entering tumor cells, we coassembled the fluorescent dye DiI into liposomes to form a DiI-labeled liposome (termed **DiI/SN38@LP**). As visualized by CLSM in Fig. 4a and quantified in Fig. 4b, **DiI/SN38@LP** gradually accumulated in the A549 cells in a time-dependent manner within 6 h. We found that the DiI signal from liposomes colocalized with the signal from lysotrackers that indicate endosomes and lysosomes, suggesting that **DiI/SN38@LP** could be effectively internalized by tumor cells. The FCM data in Fig. 4c and d further confirmed the time-dependent and effective accumulation of **DiI/SN38@LP** in tumor cells.

The uptake mechanism of prodrug-based liposomes in A549 cells was further investigated. We first explored whether the internalization of **DiI/SN38@LP** into cells is active transport dominated and energy dependent. We incubated A549 cells with **DiI/SN38@LP** at 37 °C or 4 °C for 2 h and detected accumulated drug in cells by CLSM and FCM. The CLSM images in Fig. 4e
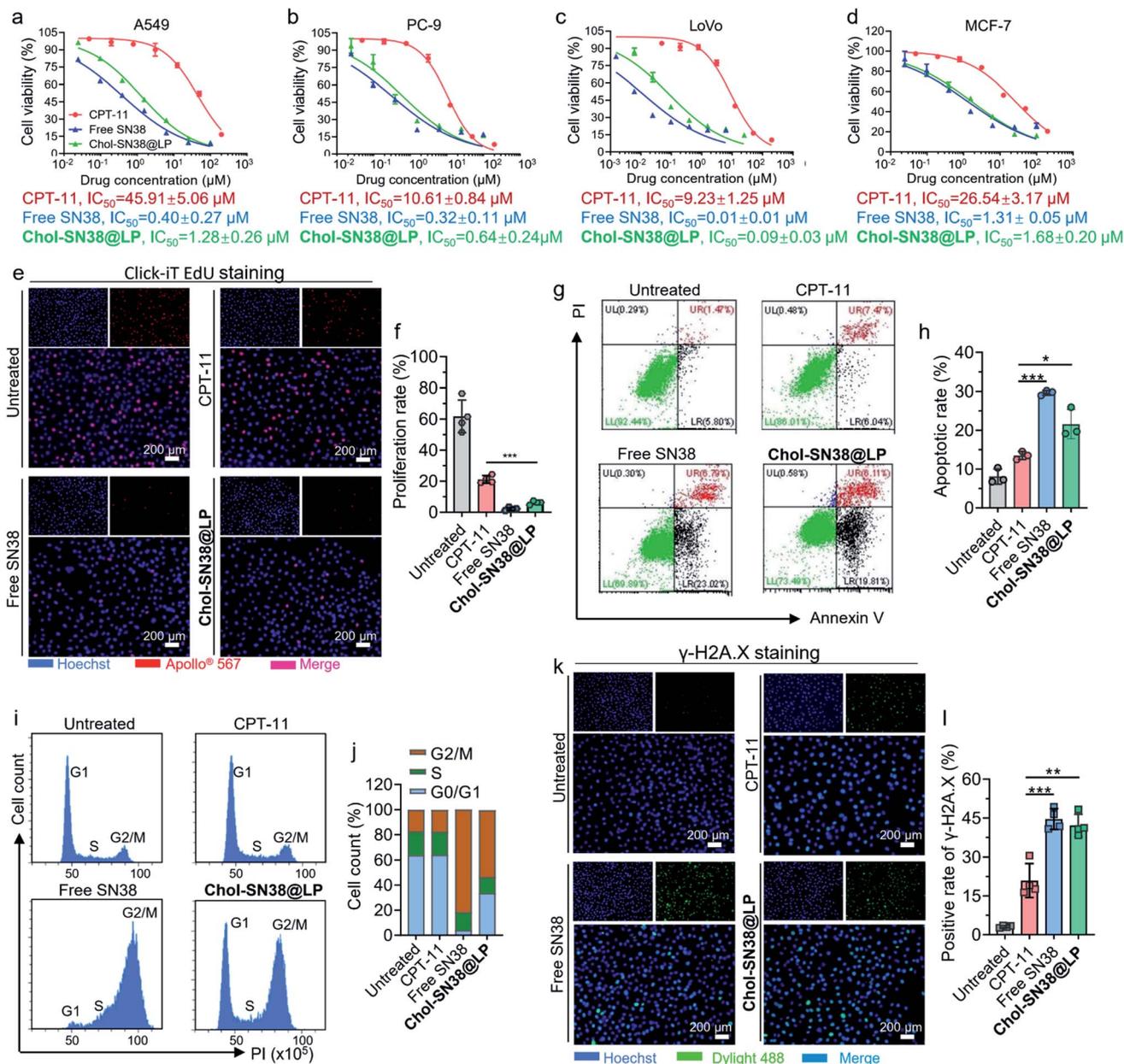
Fig. 3 *In vitro* cytotoxicity evaluation of **Chol-SN38@LP** and mechanistic analysis. Cell cytotoxicity evaluation of **Chol-SN38@LP** in A549 (a), PC-9 (b), LoVo (c) and MCF-7 (d) cell lines. The half inhibitory concentration (IC_{50}) of drugs on cell viability is presented below the graph. (e) EdU (5-ethynyl-2′-deoxyuridine) staining of A549 cells after 24 h of drug treatment (6 μM, SN38 equiv.). The proliferating cells were stained with Apollo® 567 (red), and cell nuclei were stained with Hoechst 33342 (blue). (f) Quantification of the proliferation rate of A549 cells from the EdU staining assay. (g) The effect of free SN38, CPT-11 and **Chol-SN38@LP** (4 μM, SN38 equiv., 48 h) on the apoptotic cell proportion in A549 cells was detected by flow cytometry. (h) Quantification of the cell apoptotic rate in A549 cells. Cell cycle pattern (i) and quantification of cell cycle distribution (j) in A549 cells after 48 h of drug administration (50 nM, SN38 equiv.). (k) Microscopy visualization of immunofluorescence-stained (γ-H2A.X) cells after 24 h of drug treatment (6 μM, SN38 equiv.). (l) The quantification of the γ-H2A.X positive expression ratio in each group.

show abundant signals from DiI-labeled liposomes in cells incubated at 37 °C, whereas no observable signal accumulated inside cells pretreated at 4 °C. The quantification of the DiI fluorescence signal indicated that the DiI signal from cells incubated at 37 °C was 35-fold higher than that at 4 °C (Fig. 4f). FCM data (Fig. 4g and h) again indicated that the decreased temperature greatly reduced the internalization efficiency of

liposomes ($p < 0.001$). We then analyzed the uptake pathway with specific endocytic inhibitors. As depicted in Fig. 4i and j, the administration of chlorpromazine (clathrin-dependent endocytosis inhibitor) significantly decreased the cellular uptake of liposomes (reduction to 9.4 ± 0.05%), while cytochalasin D (pinocytosis inhibitor) and filipin (caveolin-mediated endocytosis inhibitor)[29–31] did not affect the internalization of **DiI/SN38@LP**.
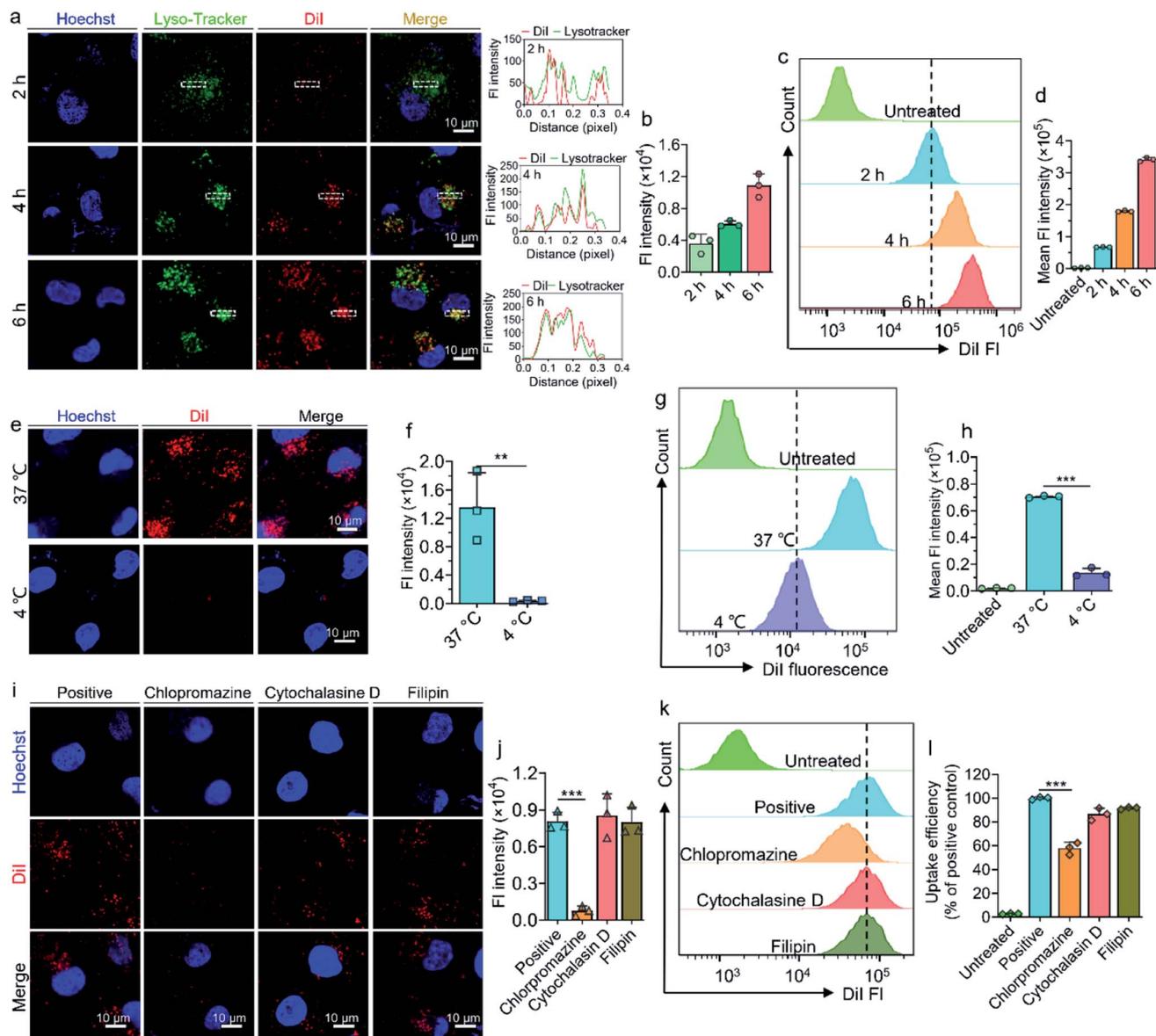
Fig. 4 Transcytotic uptake and uptake mechanism of liposomes in A549 cells. (a) Confocal laser scanning microscopy (CLSM) images of the cellular uptake of DiI-loaded liposomes in A549 cells. Cells were treated with liposomes for 2, 4 and 6 h before visualization by CLSM. The cell nuclei and lysosomes were stained with Hoechst 33342 (blue) and LysoTracker Green NDN-26 (green) before observation. The curves in the right panel represent the fluorescence intensities of DiI (red) and LysoTracker Green NDN-26 (green). (b) Quantification of the average DiI fluorescence intensity observed by CLSM in A549 cells. (c) Flow cytometry (FCM) analysis of cellular uptake of DiI-loaded liposomes by A549 cells and quantification of fluorescence intensity (d). CLSM observation (e) and quantification (f) of cellular uptake of liposomes upon 2 h of incubation with liposomes at 4 °C or 37 °C. FCM analysis (g) and quantification (h) of cellular uptake of DiI/SN38@LP at 4 °C or 37 °C. CLSM images (i) and quantification (j) of cellular uptake of liposomes when the cells were preincubated with inhibitors including chlorpromazine, cytochalasin D and filipin for 1 h. FCM data (k) and quantification (l) of cellular internalization of DiI-loaded liposomes upon preincubation with three endocytosis inhibitors. Fl: fluorescence.

The FCM analysis presented in Fig. 4k and l also confirmed that only chlorpromazine significantly decreased the cellular endocytosis of nanoparticles ($p < 0.001$). We can conclude from these results that the internalization of prodrug-based liposomes into cells occurs *via* an active, energy-consuming and clathrin-dependent endocytotic pathway.

3.6. Biodistribution of Chol-SN38@LP

We next investigated the behavior of liposomes after systemic administration in an A549 cell-derived xenograft tumor mouse model. As shown in Fig. 5a, NIR fluorescence, DiR, was coassembled into liposomes to form DiR-labeled liposome **DiR/SN38@LP** to track the biodistribution of the platform. 24 h and 48 h after intravenous administration of free DiR and **DiR/**
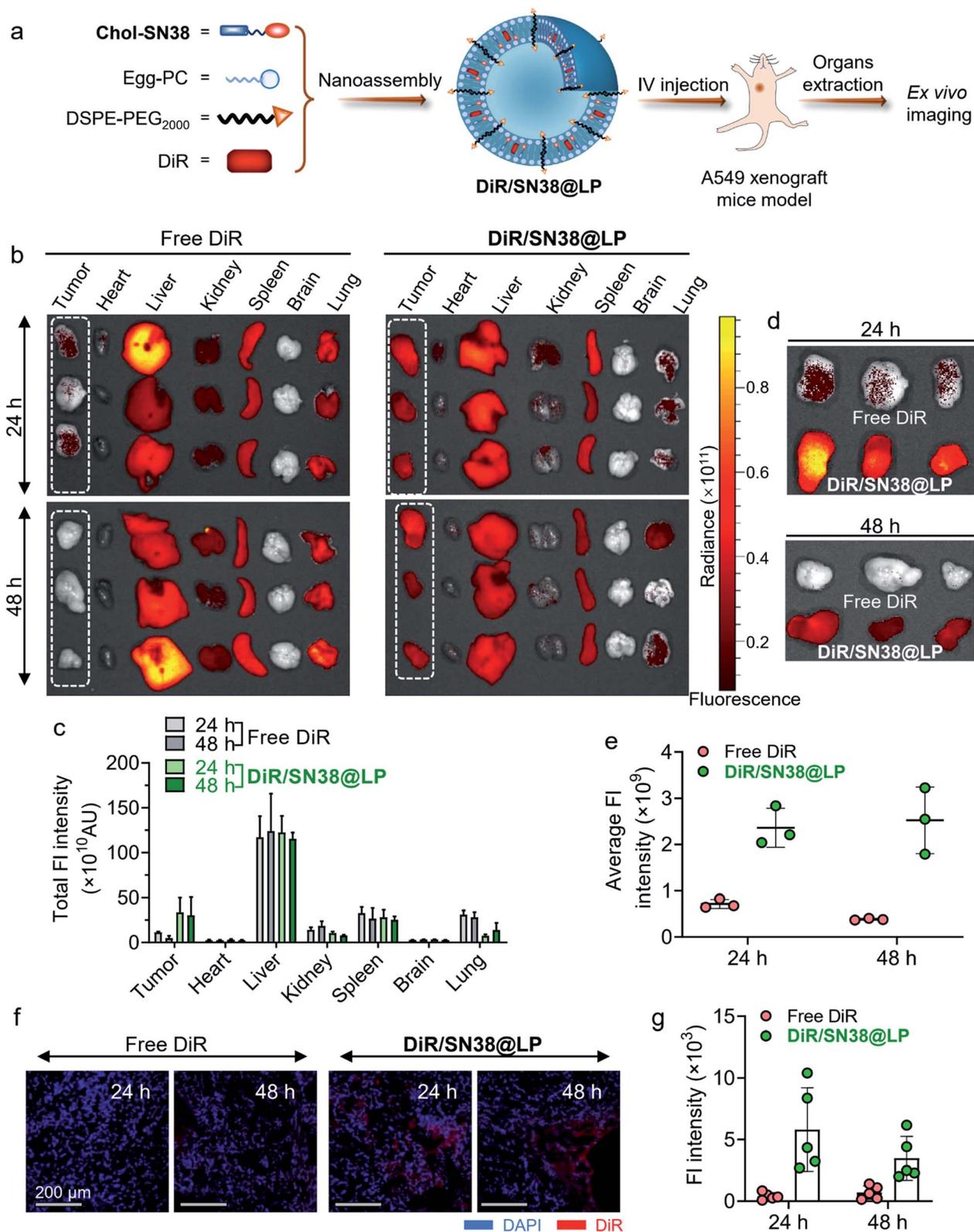
Fig. 5 Analysis of the biodistribution of prodrug-based liposomes by *ex vivo* imaging. (a) Construction of DiR-loaded liposomes (termed DiR/SN38@LP) to track the distribution of liposomes in the A549 xenograft mouse model. (b) *Ex vivo* imaging of major organs (including heart, liver, kidney, spleen, brain and lung) and tumors collected from the A549 xenograft mouse model at 24 and 48 h post administration of free DiR and DiR/SN38@LP. (c) Quantification of the fluorescence (Fl) signal from DiR in various organs and tumors. (d) *Ex vivo* imaging of tumors extracted at 24 and 48 h post administration of two formulations of DiR. (e) The average DiR Fl intensity in tumors at both time points. (f) CLSM observation of the distribution of DiR-loaded liposomes in tumor sections. (g) Quantification of DiR Fl intensity from CLSM observations.
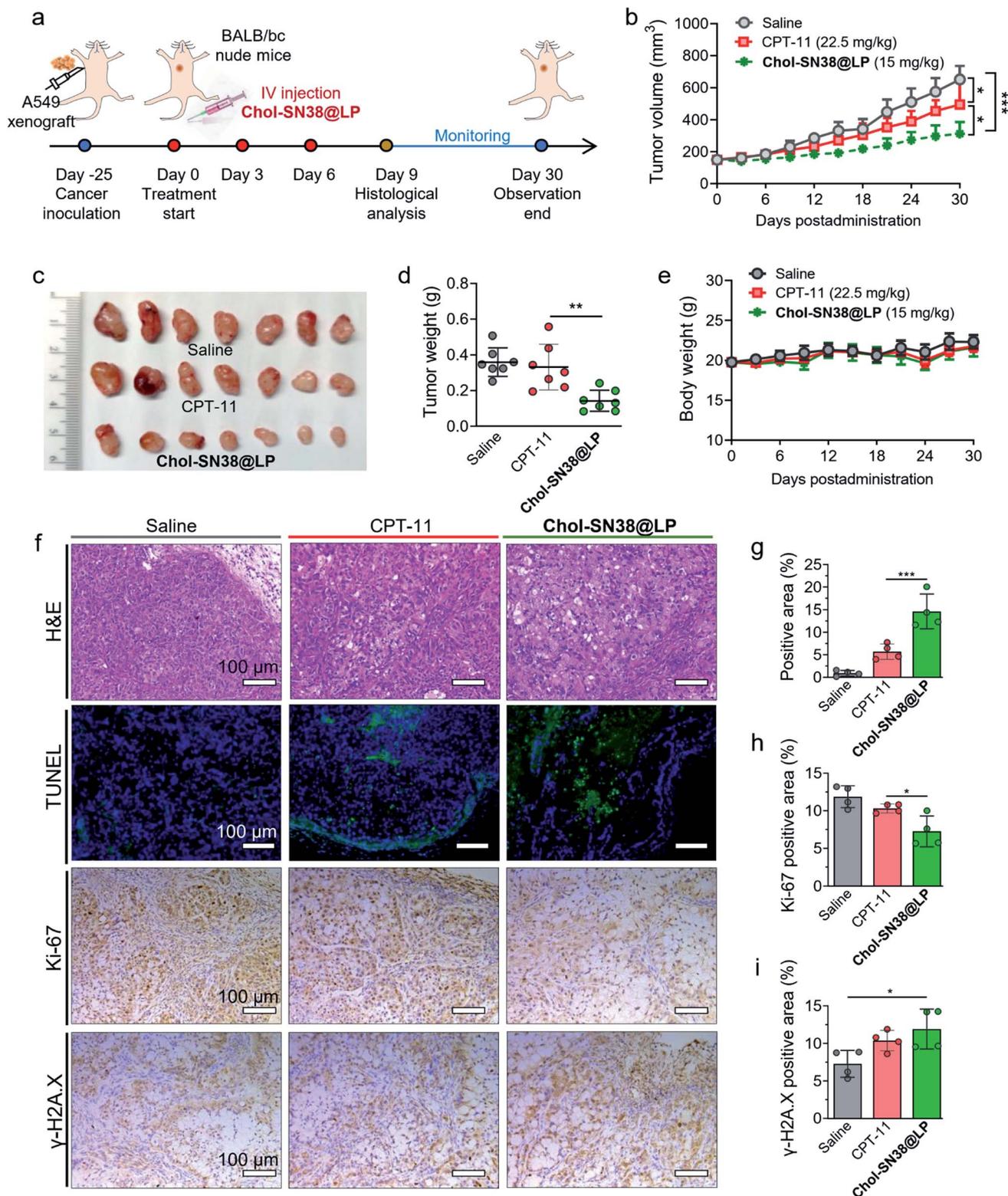
Fig. 6 *In vivo* antitumor efficacy of liposomal nanomedicines in an A549 xenograft mouse model. (a) The overall schedule of subcutaneous A549 mouse model establishment and drug administration. Mice ($n = 7$) bearing A549 tumors were intravenously treated with saline, CPT-11 or **Chol-SN38@LP** (15 mg kg^{-1} SN38 equiv.) every three days three times. The tumor size and body weight were recorded from day 0 to the end of observation at day 30. (b) The tumor growth curves of mice in each group. Photographs of the excised tumors in each group at the end of the experiment (c) and the tumor weight of excised tumors (d). (e) Body weight variation throughout treatment. Representative H&E staining, immunofluorescence staining (TUNEL) and immunohistological staining (Ki-67 and γ-H2A.X) of tumors excised at day 9 (f). The quantification of positive area ratio of TUNEL (g), Ki-67 (h) and γ-H2A.X (i).

SN38@LP, major organs and tumors were extracted for *ex vivo* imaging to detect the biodistribution and tumor targeting capability. As revealed in Fig. 5b and quantified in Fig. 5c, the NIR signal of tumors from mice receiving prodrug-based liposomal DiR was higher than that of other organs except for liver and spleen. In sharp contrast, the NIR signal was highly distributed in the liver, spleen, lung and kidney but rarely accumulated in tumors from free DiR-administered mice at both 24 h and 48 h. The rearrangement of tumors together in Fig. 5d clearly presented the large difference in distribution between those two formulations. The NIR signal from tumors with liposomal treatment was 3.3 and 6.6 times stronger than that of free DiR administration (Fig. 5e) at 24 h and 48 h post administration, further supporting that the DiR signal was quickly metabolized and eliminated in mice treated with the free formulation of DiR while being maintained at a high level for up to 48 h post injection of **DiR/SN38@LP**. We further explored drug distribution in tumors histologically and visualized by CLSM. Compared to the rarely detectable DiR signals derived from tumor sections in the free DiR-treated group, the strong NIR signals (red) were distributed in tumor tissues from mice treated with **DiR/SN38@LP** (Fig. 5f and g). Together, these results verified the tumor-specific long-term targeting ability of this prodrug-based liposomal scaffold.

3.7. *In vivo* antitumor activity in an A549 cell-derived xenograft tumor mouse model

Encouraged by the excellent performance of our prodrug-based liposomal platform in cytotoxicity and *in vivo* tumor-specific targeting, we further evaluated the therapeutic efficacy of this nanoformulation in a preclinical mouse model bearing subcutaneous A549 xenografts in BALB/c nude mice. The experimental protocol is shown in Fig. 6a. The mice were intravenously administered CPT-11 or **Chol-SN38@LP** (15 mg kg^{-1} SN38 equiv. dose, q3d × 3) when the tumor volume reached approximately 150 mm^3. As shown in Fig. 6b, three injections of nanoparticles significantly delayed tumor growth, while the tumors in mice treated with saline and CPT-11 experienced a surge increase during the observation period. The average tumor size in the **Chol-SN38@LP**-treated group was ∼48.0%, and 63.2% of the tumor size in the saline- and CPT-11-administered groups at day 30. Tumors excised from **Chol-SN38@LP**-treated mice at the endpoint of observation were apparently smaller than those from mice treated with saline and CPT-11 (Fig. 6c). The average tumor weights from the saline and CPT-11 groups were ∼2.5 and 2.3 times of magnitude higher than those from the liposomal formulation group (Fig. 6d). Encouragingly, no visible body weight variations occurred after three **Chol-SN38@LP** injections, implying that this formulation had no severe *in vivo* toxicity in mice (Fig. 6e).

A representative primary tumor in each group was collected on day 9 for histological analysis. H&E staining and TUNEL assay of tumors were in accordance with the above-observed tumor reduction and clearly revealed that **Chol-SN38@LP** resulted in extensive intratumoral apoptosis (Fig. 6f). The quantification of the positive signal (from apoptotic body) ratio in tumor sections by

TUNEL staining (Fig. 6g) shows that compared to CPT-11 treatment, **Chol-SN38@LP** treatment rendered a 2.6-fold increase in tumor cellular apoptosis. IHC staining of the proliferation marker Ki-67 and the quantification of the positive staining area (Fig. 6f and h) showed that compared to saline and CPT-11 treatment, the prodrug-based nanoparticulate platform caused ∼1.6- and 1.4-fold reductions in tumor proliferation in tumor tissues, respectively. The γ-H2A.X staining of tumor sections revealed that in comparison with saline and CPT-11 treatment, **Chol-SN38@LP** administration considerably increased the expression level of γ-H2A.X in tumor cells, suggesting that the liposomal platform could efficiently release the active therapeutic SN38 to exert potent DNA-damaging effects on tumor cells (Fig. 6f and i).

3.8. Alleviating SN38 toxicity by exploiting the drug delivery of prodrug-loaded liposomes

Repeated administration of CPT-11 in clinical practice induces severe gastrointestinal (GI) toxicity (*i.e.*, diarrhea) and hepatorenal toxicity in patients.[32,33] Here, we hypothesized that our prodrug-based liposomal strategy has the potential to alleviate bloody diarrhea and hepatorenal damage caused by CPT-11. As shown in Fig. 7a, we used healthy ICR mice to carefully evaluate whether our liposomes could prevent the incidence of bloody diarrhea and reduce the toxicity to other organs. Mice were intravenously injected with saline, CPT-11 or **Chol-SN38@LP** (15 mg kg^{-1} of SN38 equivalent dose) on days 0, 2 and 4. At 7 days post administration, organs and serum were collected from mice to assess drug toxicity to organs and to hepatorenal functions, respectively. As shown in Fig. 7b, mice ($n = 8$) receiving CPT-11 treatment experienced diarrhea and peaked at day 4, with all diarrhea severity scores increasing to 2 and 3. However, mice treated with SN38 prodrug-loaded liposomes suffered less bloody diarrhea severity at all observation times, with no diarrhea score over grade 2. The results from H&E staining of the ileum in Fig. 7c revealed that CPT-11 injection caused apparent villus atrophy in the ileum, while the ileum remained healthy in mice receiving **Chol-SN38@LP** treatment.

The toxicity to the liver and kidney was further examined by measuring a series of serological markers that indicate hepatorenal function. In comparison with saline-administered mice, the mice ($n = 6$) that were treated with CPT-11 experienced a significant elevation in the hepatic parameter aspartate aminotransferase (AST) in the serum ($p < 0.05$), which indicates potentially acute toxicity to the liver (Fig. 7d). In contrast, no significant elevation of hepatorenal function indices was noted following the treatments of **Chol-SN38@LP** (Fig. 7e–h). The result from the H&E staining of the liver is in agreement with the data from serological testing, revealing that CPT-11 induced severe hepatocellular apoptosis, while no lesions were found in livers from mice treated with **Chol-SN38@LP** (Fig. 7i). **Chol-SN38@LP** also showed no harm to other major organs as analyzed by H&E staining (Fig. S5†). Collectively, these results demonstrated that our nanomedicine can alleviate *in vivo* toxicity caused by CPT-11, including bloody diarrhea, intestinal damage and liver injury, thereby implying its potential as a clinical candidate for the upgrading and replacement of CPT-11 or other camptothecin derivates.
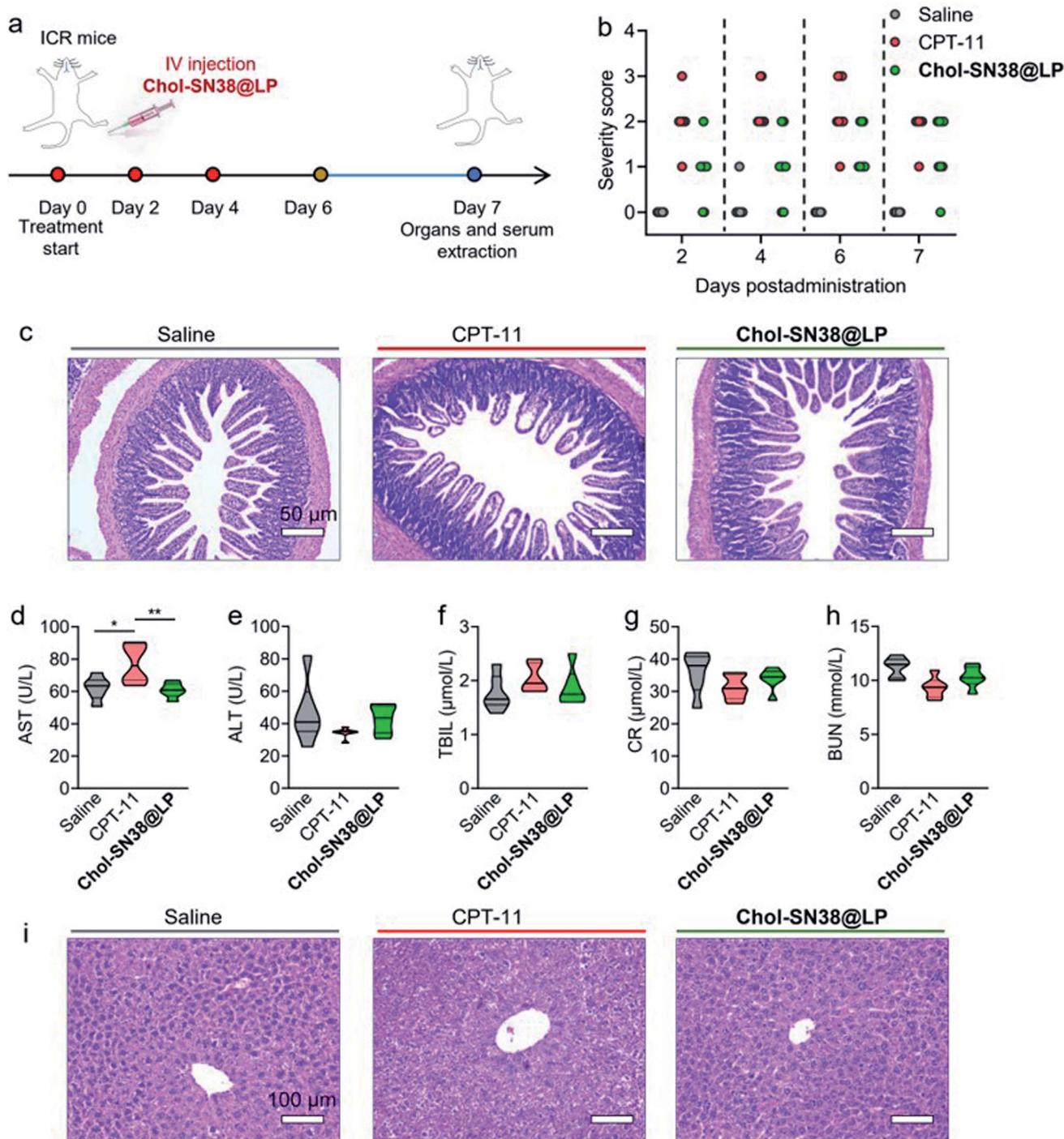
Fig. 7 *In vivo* toxicity evaluation of **Chol-SN38@LP** in ICR mice. (a) Drug administration schedule in ICR mice for assessing *in vivo* toxicity. **Chol-SN38@LP** and CPT-11 were injected on days 0, 2 and 4. (b) The severity score of bloody diarrhea in mice at days 2, 4, 6 and 7. (c) H&E staining images of ileum collected at 7 days post administration to determine the toxicity of liposomes to intestines. Analysis of hepatorenal function indices, including aspartate aminotransferase (AST) (d), alanine aminotransferase (ALT) (e), total bilirubin (TBIL) (f), creatinine (CR) (g) and blood urea nitrogen (BUN) (h), in ICR mice 7 days post drug administration. (i) H&E staining images of liver extracted from mice at day 7.

4. Discussion

SN38, an active metabolite of CPT-11, has attracted much attention from researchers for its potent efficacy in inducing cell apoptosis relative to its parent drug CPT-11 and decreased inefficient drug conversion from CPT-11 to SN38.[2,4] However, studies and clinical translation of SN38 have been greatly comprised because of its poor solubility in water and extremely low affinity with nanocarriers. Thus, re-engineering the architecture of SN38 for prodrug reconstitution to self-assemble in

water or coassemble with nanocarriers is expected to overcome these challenges.[34,35]

Pioneer studies revealed that the conjugation of chemotherapeutics with lipids (*i.e.*, DHA, cholesterol or squalene) could significantly increase the miscibility of drugs with liposomal scaffolds.[9,16,36] Enlightened by those endeavors, we chose the lipid cholesterol for SN38 prodrug construction and further encapsulation with liposomal scaffolds for drug delivery. Cholesterol was carefully chosen to be covalently conjugated to SN38 because cholesterol conjugation can increase cellular uptake by binding with lipoproteins and targeting overexpressed low-density lipoprotein (LDL) receptors on cancer cells.[18,37] Cancerous cells require cholesterol for their rapid growth and metabolism.[38] In addition, cholesterol conjugation can adjust the planar structure of SN38 and the affinity to liposomal carriers, enabling the stable delivery of nanomedicines in the blood circulation.[39] Further formulating liposomes with PEG functionalities on the surface ensures the reduced blood clearance in RES and long-term blood circulation of our platform.[21,22]

The SN38 prodrug in the present study was generated by esterifying the hydroxyl group of both SN38 and cholesterol with succinic acid, leading to a chemical structure that is highly hyperreactive to the esterase that is highly expressed in cancerous cells.[40] Once the prodrug-loaded liposomes are internalized into cells, the chemically unmodified active SN38 agent is specifically and efficiently released upon the catalysis of abundant esterase in tumor cells. The release profiles clearly demonstrated that exposure to PLE substantially accelerated drug release from prodrug-loaded liposomes (**Chol-SN38@LP**), suggesting that the esterase-activated release of active SN38 compound plays an essential role in exerting cytotoxic effects of this platform in intracellular conditions. Less cytotoxic activity to free SN38 but higher cytotoxicity than CPT-11 presented by **Chol-SN38@LP** in cell-based data is in accordance with the *in vitro* drug release features that drug release from nanotherapies is esterase-activatable and requires cleavage of chemical ester bonds to regain antitumor activity.

The chemical derivation of SN38 and subsequent encapsulation in liposomal scaffolds ensures sustained drug release in blood circulation, thereby ensuring efficient passive targeting to tumor lesions by the EPR effect exclusively possessed by small nanomedicines.[41] The drug distribution analysis of our liposomal strategy using fluorescence imaging clearly showed the specific and efficient accumulation of nanomedicines in tumors and was rarely distributed in other major organs except for the liver and spleen. The abundant tumor accumulation of liposomal formulations relative to the free drug formulation further explains the superior antitumor efficacy of these nanomedicines compared with solution-based free CPT-11 in a preclinical lung cancer cell A549-derived xenograft mouse model. Notably, the effective antitumor therapeutic CPT-11 in colorectal cancer treatment has shown limited and marginal tumoricidal effects in lung cancers compared to saline treatment, corresponding to the limited clinical application of CPT-11 in lung cancers.[42] The supreme antitumor efficacy of our platform offers us a clue for designing more effective systems for SN38 or other camptothecin derivates for lung cancers.

The clinical administration of the SN38 prodrug CPT-11 is reported to cause diarrhea in up to 70% of treated patients, and 31% of patients experience grade 3 or 4 diarrhea.[43] The major cause of diarrhea is that SN38 metabolized from CPT-11 is transformed into inactive SN38G in the liver and is excreted to the GI tract, where SN38G regains its active form SN38 under catalysis by β-glucuronidase enzymes from the commensal microbiota.[44] Several strategies, including the use of antibiotics to remove GI bacteria and inhibitors of β-glucuronidase,[45,46] have been found to alleviate toxicity induced by CPT-11. However, the additional administration of these agents could result in extra side effects (*i.e.*, imbalance of the gut microbiome and intestinal dysfunction) in patients, which may pose a huge burden for cancer patients. As a result, reducing the total amount of free SN38 accumulated in the intestines seems to be a more rational and practical approach to alleviate drug-associated toxicity. Impressively, our liposomal formulation of SN38 significantly decreased the incidence and severity of bloody diarrhea as well as less intestinal damage in mice than CPT-11. Thus, the systemic side effects induced by clinical CPT-11 could be largely diminished by rational design and exploitation of smart nanoparticle strategies for SN38 delivery.

In conclusion, our approach combines rational prodrug reconstitution with subsequent encapsulation in liposomal scaffolds for the construction of chemotherapeutic SN38-based nanomedicines for the treatment of lung cancer. Compared with the clinically commonly used SN38 prodrug CPT-11, our SN38-based nanoparticle system achieved a markedly improved therapeutic efficacy and safety profile because of (1) sustained drug release and prolonged circulation ensured by the higher affinity of lipid formulated prodrug with the liposomal carrier; (2) specific esterase-responsive cleavage of the prodrug in tumor cells; (3) increased internalization of the system into cancer cells due to cholesterol conjugation; and (4) efficient targeting to *in situ* tumor lesions by the EPR effect. We believe that our platform has great potential for applications to rescue other potent therapeutic candidates that have failed in clinical trials because of poor PK properties or uncertain safety in patients.

Conflicts of interest

The authors declare no potential conflicts of interest.

Acknowledgements

References

1 P. Sapra, H. Zhao, M. Mehlig, J. Malaby, P. Kraft, C. Longley, L. M. Greenberger and I. D. Horak, Novel delivery of SN38 markedly inhibits tumor growth in xenografts, including

a camptothecin-11 - refractory model, *Clin. Cancer Res.*, 2008, **14**, 1888–1896.

2 H. Wang, H. Xie, J. Wu, X. Wei, L. Zhou, X. Xu and S. Zheng, Structure-Based Rational Design of Prodrugs To Enable Their Combination with Polymeric Nanoparticle Delivery Platforms for Enhanced Antitumor Efficacy, *Angew. Chem.*, 2014, **53**, 11532–11537.

3 W. Han, L. Shi, B. Xie, J. Wan, L. Ren, Y. Wang, X. Chen and H. Wang, Supramolecular Engineering of Molecular Inhibitors in an Adaptive Cytotoxic Nanoparticle for Synergistic Cancer Therapy, *ACS Appl. Mater. Interfaces*, 2020, **12**, 1707–1720.

4 Y. Wang, H. Xie, K. Ying, B. Xie and H. Wang, Tuning the efficacy of esterase-activatable prodrug nanoparticles for the treatment of colorectal malignancies, *Biomaterials*, 2021, 120705.

5 H. Wang, L. Zhou, K. Xie, J. Wu, P. Song, H. Xie, L. Zhou, J. Liu, X. Xu, Y. Shen and S. Zheng, Polylactide-tethered prodrugs in polymeric nanoparticles as reliable nanomedicines for the efficient eradication of patient-derived hepatocellular carcinoma, *Theranostics*, 2018, **8**, 3949–3963.

6 J. G. Slatter, L. J. Schaaf, J. P. Sams, K. L. Feenstra and R. S. Lord, Pharmacokinetics, Metabolism, and Excretion of Irinotecan (CPT-11) Following I.V. Infusion of [14C]CPT-11 in Cancer Patients, *Drug Metab. Dispos.*, 2000, **28**, 423–433.

7 E. Gupta, T. M. Lestingi, R. Mick, J. Ramirez, E. E. Vokes and M. J. Ratain, Metabolic fate of irinotecan in humans: correlation of glucuronidation with diarrhea, *Cancer Res.*, 1994, **54**, 3723–3725.

8 I. F. Tannock, C. M. Lee, J. K. Tunggal, D. S. Cowan and M. J. Egorin, Limited penetration of anticancer drugs through tumor tissue: a potential cause of resistance of solid tumors to chemotherapy, *Clin. Cancer Res.*, 2002, **8**, 878–884.

9 L. Shi, Y. Wang, Q. Wang, Z. Jiang, L. Ren, Y. Yan, Z. Liu, J. Wan, L. Huang, B. Cen, W. Han and H. Wang, Transforming a toxic drug into an efficacious nanomedicine using a lipoprodrug strategy for the treatment of patient-derived melanoma xenografts, *J. Controlled Release*, 2020, **324**, 289–302.

10 T. M. Allen and P. R. Cullis, Liposomal drug delivery systems: from concept to clinical applications, *Adv. Drug Delivery Rev.*, 2013, **65**, 36–48.

11 A. K. Awasthi, S. Gupta, J. Thakur, S. Gupta, S. Pal, A. Bajaj and A. Srivastava, Polydopamine-on-liposomes: stable nanoformulations, uniform coatings and superior antifouling performance, *Nanoscale*, 2020, **12**, 5021–5030.

12 Y. Barenholz, Doxil (R) - The first FDA-approved nano-drug: lessons learned, *J. Controlled Release*, 2012, **160**, 117–134.

13 C. M. Dawidczyk, C. Kim, J. H. Park, L. M. Russell, K. H. Lee, M. G. Pomper and P. C. Searson, State-of-the-art in design rules for drug delivery platforms: lessons learned from FDA-approved nanomedicines, *J. Controlled Release*, 2014, **187**, 133–144.

14 N. Filipczak, J. Y. Pan, S. S. K. Yalamarty and V. P. Torchilin, Recent advancements in liposome technology, *Adv. Drug Delivery Rev.*, 2020, **156**, 4–22.

15 U. Bulbake, S. Doppalapudi, N. Kommineni and W. Khan, Liposomal Formulations in Clinical Use: An Updated Review, *Pharmaceutics*, 2017, **9**, 1–33.

16 F. Tao, Y. Dong, X. Zhang, X. Ke and H. Wang, Integrating a novel SN38 prodrug into the PEGylated liposomal system as a robust platform for efficient cancer therapy in solid tumors, *Int. J. Pharm.*, 2016, **512**, 39–48.

17 K. Xie, S. Song, L. Zhou, J. Wan, Y. Qiao, M. Wang, H. Xie, L. Zhou, S. Zheng and H. Wang, Revival of a potent therapeutic maytansinoid agent using a strategy that combines covalent drug conjugation with sequential nanoparticle assembly, *Int. J. Pharm.*, 2019, **556**, 159–171.

18 A. Radwan and F. K. Alanazi, Targeting cancer using cholesterol conjugates, *Saudi Pharm. J.*, 2014, **22**, 3–16.

19 D. Yang, W. Wang, M. Feng, W. Yu, J. Zhou, X. Ding, Z. Xin, C. Liu, R. Wang and Q. Zhang, A biomimetic nanovector-mediated targeted cholesterol-conjugated siRNA delivery for tumor gene therapy, *Biomaterials*, 2012, **33**, 8893–8905.

20 A. Radwan and F. Alanazi, Design and synthesis of new cholesterol-conjugated 5-Fluorouracil: a novel potential delivery system for cancer treatment, *Molecules*, 2014, **19**, 13177–13187.

21 A. Kolate, D. Baradia, S. Patil, I. Vhora, G. Kore and A. Misra, PEG — A versatile conjugating ligand for drugs and drug delivery systems, *J. Controlled Release*, 2014, **192**, 67–81.

22 J. S. Suk, Q. G. Xu, N. Kim, J. Hanes and L. M. Ensign, PEGylation as a strategy for improving nanoparticle-based drug and gene delivery, *Adv. Drug Delivery Rev.*, 2016, **99**, 28–51.

23 H. Kang, S. Rho, W. R. Stiles, S. Hu, Y. Baek, D. W. Hwang, S. Kashiwagi, M. S. Kim and H. S. Choi, Size-Dependent EPR Effect of Polymeric Nanoparticles on Tumor Targeting, *Adv. Healthcare Mater.*, 2020, **9**, e1901223.

24 J. Fang, W. Islam and H. Maeda, Exploiting the dynamics of the EPR effect and strategies to improve the therapeutic effects of nanomedicines by using EPR effect enhancers, *Adv. Drug Delivery Rev.*, 2020, **157**, 142–160.

25 V. Bala, S. S. Rao, B. J. Boyd and C. A. Prestidge, Prodrug and nanomedicine approaches for the delivery of the camptothecin analogue SN38, *J. Controlled Release*, 2013, **172**, 48–61.

26 V. Bottero, V. Busuttil, A. Loubat, N. Magne, J. L. Fischel, G. Milano and J. F. Peyron, Activation of nuclear factor kappa B through the IKK complex by the topoisomerase poisons SN38 and doxorubicin: A brake to apoptosis in HeLa human carcinoma cells, *Cancer Res.*, 2001, **61**, 7785–7791.

27 A. Xiao, H. T. Li, D. Shechter, S. H. Ahn, L. A. Fabrizio, H. Erdjument-Bromage, S. Ishibe-Murakami, B. Wang, P. Tempst, K. Hofmann, D. J. Patel, S. J. Elledge and C. D. Allis, WSTF regulates the H2A.X DNA damage response *via* a novel tyrosine kinase activity, *Nature*, 2009, **457**, 57–62.

28 P. Sandra, P. Le. Florent, B. Siau-Kun, C. Odile and A. Salomé, The Histone Chaperone FACT Coordinates H2A.X-Dependent Signaling and Repair of DNA Damage, *Mol. Cell*, 2018, **72**, 888–901.

29 J. Wan, L. Huang, J. Cheng, H. Qi, J. Jin and H. Wang, Balancing the stability and drug activation in adaptive nanoparticles potentiates chemotherapy in multidrug-resistant cancer, *Theranostics*, 2021, **11**, 4137–4154.

30 D. Vercauteren, R. E. Vandenbroucke, A. T. Jones, J. Rejman, J. Demeester, S. C. De Smedt, N. N. Sanders and K. Braeckmans, The Use of Inhibitors to Study Endocytic Pathways of Gene Carriers: Optimization and Pitfalls, *Mol. Ther.*, 2010, **18**, 561–569.

31 M. Lopes, N. Shrestha, A. Correia, M. A. Shahbazi, B. Sarmento, J. Hirvonen, F. Veiga, R. Seica, A. Ribeiro and H. A. Santos, Dual chitosan/albumin-coated alginate/dextran sulfate nanoparticles for enhanced oral delivery of insulin, *J. Controlled Release*, 2016, **232**, 29–41.

32 Q. Lian, J. Xu, S. Yan, M. Huang, H. Ding, X. Sun, A. Bi, J. Ding, B. Sun and M. Geng, Chemotherapy-induced intestinal inflammatory responses are mediated by exosome secretion of double-strand DNA *via* AIM2 inflammasome activation, *Cell Res.*, 2017, **27**, 784–800.

33 X. Liu, A. Situ, Y. Kang, K. R. Villabroza, Y. Liao, C. H. Chang, T. Donahue, A. E. Nel and H. Meng, Irinotecan Delivery by Lipid-Coated Mesoporous Silica Nanoparticles Shows Improved Efficacy and Safety over Liposomes for Pancreatic Cancer, *ACS Nano*, 2016, **10**, 2702–2715.

34 J. Liang, H. Wang, W. Ding, J. Huang, X. Zhou, H. Wang, X. Dong, G. Li, E. Chen, F. Zhou, H. Fan, J. Xia, B. Shen, D. Cai, P. Lan, H. Jiang, J. Ling, Z. Cheng, X. Liu and J. Sun, Nanoparticle-enhanced chemo-immunotherapy to trigger robust antitumor immunity, *Sci. Adv.*, 2020, **6**, eabc3646.

35 W. Han, B. Xie, Y. Li, L. Shi, J. Wan, X. Chen and H. Wang, Orally Deliverable Nanotherapeutics for the Synergistic Treatment of Colitis-Associated Colorectal Cancer, *Theranostics*, 2019, **9**, 7458–7473.

36 P. J. Stevens, M. Sekido and R. J. Lee, A folate receptor-targeted lipid nanoparticle formulation for a lipophilic paclitaxel prodrug, *Pharm. Res.*, 2004, **21**, 2153–2157.

37 L. Maletínská, E. A. Blakely, K. A. Bjornstad, D. F. Deen, L. J. Knoff and T. M. Forte, Human glioblastoma cell lines: levels of low-density lipoprotein receptor and low-density lipoprotein receptor-related protein, *Cancer Res.*, 2000, **60**, 2300–2303.

38 G. R. Villa, J. J. Hulce, C. Zanca, J. Bi, S. Ikegami, G. L. Cahill, Y. Gu, K. M. Lum, K. Masui, H. Yang, X. Rong, C. Hong, K. M. Turner, F. Liu, G. C. Hon, D. Jenkins, M. Martini, A. M. Armando, O. Quehenberger, T. F. Cloughesy, F. B. Furnari, W. K. Cavenee, P. Tontonoz, T. C. Gahman, A. K. Shiau, B. F. Cravatt and P. S. Mischel, An LXR-Cholesterol Axis Creates a Metabolic Co-Dependency for Brain Cancers, *Cancer Cell*, 2016, **30**, 683–693.

39 K. C. Mei, Y. P. Liao, J. Jiang, M. Chiang, M. Khazaieli, X. Liu, X. Wang, Q. Liu, C. H. Chang, X. Zhang, J. Li, Y. Ji, B. Melano, D. Telesca, T. Xia, H. Meng and A. E. Nel, Liposomal Delivery of Mitoxantrone and a Cholesteryl Indoximod Prodrug Provides Effective Chemo-immunotherapy in Multiple Solid Tumors, *ACS Nano*, 2020, **14**, 13343–13366.

40 A. Romeo, P. C. Sanchez-Diaz, W. E. Haskins, G. E. Tomlinson and J. Y. Hung, Abstract 5144: Ubiquitin carboxy-terminal esterase L1 (UCHL1) in stem-like cancer cells of embryonal neural tumors, *Cancer Res.*, 2010, **70**, 5144.

41 J. Fang, H. Nakamura and H. Maeda, The EPR effect: Unique features of tumor blood vessels for drug delivery, factors involved, and limitations and augmentation of the effect, *Adv. Drug Delivery Rev.*, 2011, **63**, 136–151.

42 R. Rosell, E. Carcereny, R. Gervais, A. Vergnenegre, B. Massuti, E. Felip, R. Palmero, R. Garcia-Gomez, C. Pallares, J. M. Sanchez, R. Porta, M. Cobo, P. Garrido, F. Longo, T. Moran, A. Insa, F. De Marinis, R. Corre, I. Bover, A. Illiano, E. Dansin, J. de Castro, M. Milella, N. Reguart, G. Altavilla, U. Jimenez, M. Provencio, M. A. Moreno, J. Terrasa, J. Munoz-Langa, J. Valdivia, D. Isla, M. Domine, O. Molinier, J. Mazieres, N. Baize, R. Garcia-Campelo, G. Robinet, D. Rodriguez-Abreu, G. Lopez-Vivanco, V. Gebbia, L. Ferrera-Delgado, P. Bombaron, R. Bernabe, A. Bearz, A. Artal, E. Cortesi, C. Rolfo, M. Sanchez-Ronco, A. Drozdowskyj, C. Queralt, I. de Aguirre, J. L. Ramirez, J. J. Sanchez, M. A. Molina, M. Taron, L. Paz-Ares, P. Grp Francais and T. Assoc Italiana Oncologia, Erlotinib *versus* standard chemotherapy as first-line treatment for European patients with advanced EGFR mutation-positive non-small-cell lung cancer (EURTAC): a multicentre, open-label, randomised phase 3 trial, *Lancet Oncol.*, 2012, **13**, 239–246.

43 L. B. Saltz, J. V. Cox, C. Blanke, L. S. Rosen, L. Fehrenbacher, M. J. Moore, J. A. Maroun, S. P. Ackland, P. K. Locker, N. Pirotta, G. L. Elfring and L. L. Miller, Irinotecan plus fluorouracil and leucovorin for metastatic colorectal cancer. Irinotecan Study Group, *N. Engl. J. Med.*, 2000, **343**, 905–914.

44 B. Valenzuela, M. González-Sales, V. Escudero, E. Navarro and J. Pérez-Ruixo, Abstract 2213: Influence of genetic polymorphism in UGT1A1, UGT1A7 and UGT1A9 on irinotecan, SN-38 and SN-38G pharmacokinetics, *Cancer Res.*, 2013, **73**, 2213.

45 B. D. Wallace, H. Wang, K. T. Lane, J. E. Scott, J. Orans, J. S. Koo, M. Venkatesh, C. Jobin, L. A. Yeh and S. Mani, Alleviating Cancer Drug Toxicity by Inhibiting a Bacterial Enzyme, *Science*, 2010, **330**, 831–835.

46 D. Flieger, C. Klassert, S. Hainke, R. Keller, R. Kleinschmidt and W. Fischbach, Phase II Clinical Trial for Prevention of Delayed Diarrhea with Cholestyramine/Levofloxacin in the Second-Line Treatment with Irinotecan Biweekly in Patients with Metastatic Colorectal Carcinoma, *Oncology*, 2007, **72**, 10–16.